QUAZI-THREE DIMENSIONAL ANALYSIS OF TEMPERATURE FIELD INSIDE THE FLOW DUCT OF AIR SOLAR HEATER

QUSAI A. MAHDI **HAROUN A.K. SHAHAD**
DEPARTEMENT OF MECHINCAL ENGINEERING /COLLAGE OF ENGINEERING
UNIVERSITY OF BABYLON
QAM_ME782000@YAHOO.COM HAKSHAHAD@YAHOO.COM

ABSTRACT

In this paper the variation of temperature field along the duct of a solar air heater is studied using specially developed a three dimensional model .The finite volume method [FVM] is used to solve the governing equations. The effect of different operating parameters is studied such as air mass flow rate, inlet air temperature and duct aspect ratio [duct height/duct width] or what is known as flow depth. It is found that as the flow depth or aspect ratio is reduced the air is more uniformly heated through the duct cross section especially at duct exit where the air temperature becomes uniform across the duct. This shown on isothermal contours map at different cross sections. It is also found that the bulk exit air temperature increases with increasing the absorber plate temperature, i.e increasing the absorber plate temperature by about 60% gives an increase in bulk air temperature by about 9.5 ^{o}C, and the bulk exit air temperature increases with reducing air mass flow rate and flow depth, i.e. the decrease of mass flow rate by (27%) increases the bulk exit air temperature by about 3.3804 ^{o}C, and reducing the flow depth by about 33.333% increases the bulk exit air temperature increases about 4.45 ^{o}C). Also the local air temperature growth [temperature along duct height at the centre line] increases with reducing the mass flow rate and flow depth. The results also show that as the inlet air temperature increases the bulk exit air temperature increases for same mass flow rate, i.e. the increase in inlet air temperature by about 10 ^{o}C gives an increase in the exit bulk air temperature by about 6.5 ^{o}C).
Key words: solar air heater, renewable energy, solar energy, flow depth.

التحليل النظري شبه ثلاثي الابعاد لدرجات الحرارة للجريان داخل مجرى لاقط هواء شمسي

الخلاصة

تم في هذا البحث دراسة التوزيع ثلاثي الأبعاد لدرجات الحرارة على طول المجرى لمسخن هواء شمسي باستخدام موديل رياضي شبه ثلاثي الأبعاد تم بناءه لهذا الغرض. وقد تم حل المعادلات الحاكمة باستخدام طريقة الحجوم المحددة لدراسة تأثير عدد من الظروف التشغيلية كالتدفق ألكتلي للهواء ، درجة حرارة الدخول و نسبة الشكل (عمق المجرى). بينت نتائج الدراسة أنة كلما قلت عمق المجرى يكون تسخين الهواء أكثر تجانسا خلال مقطع المجرى وخصوصا في منطقة الخروج حيث تصبح درجة حرارة الهواء منتظمة تقريبا خلال المقطع وقد تم توضيح ذلك من خلال المخططات الكنتورية ولمقاطع مختلفة .وكذلك وجد أن درجه الحرارة الإجمالية تزداد بزيادة درجة حرارة اللوح الماص (أي زيادة درجة حرارة اللوح الماص بمقدار ٦٠% ووجد أن درجه الحرارة الإجمالية تزداد في المخرج بمقدار^{o}C 9.5) وكلما قل التدفق ألكتلي وعمق المجرى (أي بمعنى خفض التدفق الكتلي بنسبة(٢٧%) تزداد درجه الحرارة الإجمالية في المخرج بمقدار^{o}C 3.3804 وان خفض عمق المجرى بحدود 33.333% تزداد درجه الحرارة الإجمالية في المخرج بمقدار^{o}C 4.4515). ان درجة حرارة الهواء على طول المحور العمودي للمجرى تزداد كلما قل التدفق ألكتلي وعمق المجرى. النتائج بينت انه كلما زادت درجة حرارة الدخول فان درجة الحرارة الإجمالية للهواء في مخرج المجرى تزداد لنفس التدفق ألكتلي (أي زيادة درجة حرارة الدخول بمقدار^{o}C 10 تزداد درجه الحرارة الإجمالية في المخرج بمقدار ^{o}C 6.5).

كلمات الدلالة: سخان هواء شمسي، طاقة متجدد ة، طاقة شمسية، عمق المجرى.

NOMENCLATURE

Symbol	Description	Units
A	Area	m^2
$C_\mu , C_{\varepsilon 1} , C_{\varepsilon 2}, C_k , C_\varepsilon$	Coefficients of turbulence model	
c_p	Specific heat at constant pressure	J/kg.K
D_h	Hydraulic diameter	m
G	Generation source	$kg.m/sec^3$
h	Convective heat transfer coefficient	$W/m^2.{}^oC$
I	Incident solar radiation	W/m^2
k	Turbulent kinetic energy	m^2/sec^2
L	Duct length	m
$\dot{m}$	Mass flow rate	kg/sec
P	Pressure	N/m^2
PP	Wetted Perimeter	m
T	Temperature	^oC
T^*	Dimensionless temperature	
u	Velocity in (x) direction	m/sec
v	Velocity in (y) direction	m/sec
w	Velocity in (z) direction	m/sec
Pr	Laminar Prandtl number	

Greek Symbols

α	Duct aspect ratio	
ε	Rate of dissipation of turbulent kinetic energyu	
μ	Fluid viscosity	kg/m.sec
ρ	Fluid density	kg/m^3
σ_k	Constant in eq. 7	
σ_ε	Constant in eq. 8	

Subscripts

b	bulk values
eff	effective
in	inlet section
l	laminar
t	turbulent

1. Introduction

Solar energy is clean, indepletable, and harmless to living organisms on the earth because the harmful short wavelength Ultraviolet Rays are absorbed before reaching the troposphere by stratospheric ozone layers and weakened by the air composition and moisture in the troposphere. Solar energy energizes the atmosphere and thus generates climatic phenomena, but the balance of energy is absorbed by molecules of the materials on the earth surface and converted in to the heat at low temperature [1]. Many significant experiments and simulations on solar collector were published, some aimed to reducing the cost and improvement the performance and efficiencies improvements. Many designs were suggested such as (single and multi-pass heater, some are of the packed type and others incorporate fins to enhance heat transfer) .

Ashish K. [2] studied theoretically the behavior of counter flow solar air heater and compared its performance with the conventional type under different operating conditions. He found that the counter flow heater is more efficient than the conventional type.

Hossien Assefi, et al [3] found that as the mass flow rate decreases the outlet temperature increases while the efficiency decreases.

Molero Villar, et al [4] developed a three dimensional transient model for analyzing the performance of a flat plate collector. Different configurations were studied such as parallel tubes collector (PTC), serpentine tube collector (STC) and two parallel plate collectors (TPPC).

Ho-Mong Yeh, et al [5] studied theoretically the effect of external recycle on collector efficiency in solar air heater. It was found that considerable improvement in collector efficiency is obtainable if the operation is carried out with external recycle.

In Iraq the use of solar energy is very attractive due to its geographical locations. Iraq lies within latitude (33^o N and longitude 44^o E). For sunny countries like Iraq the potential for developing solar energy technology is great. Thus, there is clearly a need for a systematic and serious studies on the performance and efficiency of solar energy system of various designs.

Nama S. et al [6] used sunshine duration and extraterrestrial radiation as input parameters in four mathematical models to estimate the daily average diffuse solar radiation in various locations of IRAQ during the period 1961-1991. It was found that the maximum value of diffuse solar radiation occurred in summer and it is in the range 2-9 MJ/m^2.day.

The aim of this work is to develop a numerical algorithm and to built a computer program to study the local and temporal temperature of air as it flows though the heater passages. The effect of absorber plate temperature, inlet air temperature, air mass flow rate, and passage configuration on temperature are studied.

2. Model Description and Assumptions

The physical model studied is shown schematically in fig. (1). It shows the main parts of the collector which are the wooden box, the absorber plate and the glass cover. The absorber plate is fabricated as an air duct. Different duct configurations are used. The working fluid (air) is allowed to flow in the duct and stagnant air is trapped between the cover and the absorber. Three different duct configurations will be used. The dimension of the first configuration (square duct) is (10x10 cm). The duct aspect ratio α, height to width ratio, is equal unity. This arrangement is the same as that employed by experimental work [7]. The aspect ratios for the second and third configurations are (1/4), and (1/11), respectively. The duct length is (4.5) m for all configurations. The flow field, temperature field and heat transfer to the air as it flows through the duct are analyzed. The governing equations are the conservations of mass, energy and momentum .The following assumptions are used in the solution of the governing equations:

1. Steady state conditions during each calculation step.
2. Incompressible, three dimensional and turbulent flow.
3. All thermo- physical properties of working fluid are considered independent of temperature.
4. Developing flow at entrance.
5. Negligible dissipated energy.
6. Negligible body forces.
7. Negligible buoyancy effect.
8. No heat generation.
9. Constant absorber plate (air duct walls) temperature.
10. Constant bottom wall temperature which is equal to atmospheric temperature.

3. Mathematical Formulation

The governing equations are the continuity, momentum and energy in addition to the k-ε model proposed by Launder and Spalding [8]. In Cartesian coordinate, the continuity, momentum, energy and turbulence equations for steady incompressible flows can be written in the following compact form, Ibrahim [9].

Continuity Equation (Mass Conservation)

$$\frac{\partial u}{\partial x}+\frac{\partial v}{\partial y}+\frac{\partial w}{\partial z}=0 \tag{1}$$

Momentum Equations:

x-direction

$$\rho\left(u\frac{\partial u}{\partial x}+v\frac{\partial u}{\partial y}+w\frac{\partial u}{\partial z}\right)=-\frac{\partial P}{\partial x}+\frac{\partial}{\partial x}\left(2\mu_{eff}\frac{\partial u}{\partial x}\right)+\frac{\partial}{\partial y}\left(\mu_{eff}\frac{\partial u}{\partial y}\right)+\frac{\partial}{\partial z}\left(\mu_{eff}\frac{\partial u}{\partial z}\right)$$
$$+\frac{\partial}{\partial y}\left(\mu_{eff}\frac{\partial v}{\partial x}\right)+\frac{\partial}{\partial z}\left(\mu_{eff}\frac{\partial w}{\partial x}\right) \tag{2}$$

Where,

$$\mu_{eff}=\mu_l+\mu_t$$

y-direction

$$\rho\left(u\frac{\partial v}{\partial x}+v\frac{\partial v}{\partial y}+w\frac{\partial v}{\partial z}\right)=-\frac{\partial P}{\partial y}+\frac{\partial}{\partial x}\left(\mu_{eff}\frac{\partial v}{\partial x}\right)+\frac{\partial}{\partial y}\left(2\mu_{eff}\frac{\partial v}{\partial y}\right)+\frac{\partial}{\partial z}\left(\mu_{eff}\frac{\partial v}{\partial z}\right)$$
$$+\frac{\partial}{\partial x}\left(\mu_{eff}\frac{\partial u}{\partial y}\right)+\frac{\partial}{\partial z}\left(\mu_{eff}\frac{\partial w}{\partial y}\right) \tag{3}$$

z-direction

$$\rho\left(u\frac{\partial w}{\partial x}+v\frac{\partial w}{\partial y}+w\frac{\partial w}{\partial z}\right)=-\frac{\partial P}{\partial z}+\frac{\partial}{\partial x}\left(\mu_{eff}\frac{\partial w}{\partial x}\right)+\frac{\partial}{\partial y}\left(\mu_{eff}\frac{\partial w}{\partial y}\right)+\frac{\partial}{\partial z}\left(2\mu_{eff}\frac{\partial w}{\partial z}\right)$$
$$+\frac{\partial}{\partial x}\left(\mu_{eff}\frac{\partial u}{\partial z}\right)+\frac{\partial}{\partial y}\left(\mu_{eff}\frac{\partial v}{\partial z}\right) \tag{4}$$

Energy Equation

The energy equation in Cartesian coordinate (x, y,z) is written as, Ibrahim [9].

$$\rho\left(u\frac{\partial T}{\partial x}+v\frac{\partial T}{\partial y}+w\frac{\partial T}{\partial z}\right)=\frac{\partial}{\partial x}\left(\frac{\mu_{eff}}{Pr_{eff}}\frac{\partial T}{\partial x}\right)+\frac{\partial}{\partial y}\left(\frac{\mu_{eff}}{Pr_{eff}}\frac{\partial T}{\partial y}\right)+\frac{\partial}{\partial z}\left(\frac{\mu_{eff}}{Pr_{eff}}\frac{\partial T}{\partial z}\right) \quad (5)$$

Where,

$$\frac{\mu_{eff}}{Pr_{eff}}=\frac{\mu_l}{Pr_l}+\frac{\mu_t}{Pr_t}$$

The Standard k-ε Model:

$$\mu_t=\rho C_\mu\frac{k^2}{\varepsilon} \quad (6)$$

$$u\frac{\partial(\rho k)}{\partial x}+v\frac{\partial(\rho k)}{\partial y}+w\frac{\partial(\rho k)}{\partial z}=\frac{\partial}{\partial x}\left(\frac{\mu_t}{\sigma_k}\frac{\partial k}{\partial x}\right)+\frac{\partial}{\partial y}\left(\frac{\mu_t}{\sigma_k}\frac{\partial k}{\partial y}\right)+\frac{\partial}{\partial z}\left(\frac{\mu_t}{\sigma_k}\frac{\partial k}{\partial z}\right)$$
$$+G-\rho\varepsilon \quad (7)$$

$$u\frac{\partial(\rho\varepsilon)}{\partial x}+v\frac{\partial(\rho\varepsilon)}{\partial y}+w\frac{\partial(\rho\varepsilon)}{\partial z}=\frac{\partial}{\partial x}\left[\frac{\mu_t}{\sigma_\varepsilon}\frac{\partial\varepsilon}{\partial x}\right]+\frac{\partial}{\partial y}\left[\frac{\mu_t}{\sigma_\varepsilon}\frac{\partial\varepsilon}{\partial y}\right]+\frac{\partial}{\partial z}\left[\frac{\mu_t}{\sigma_\varepsilon}\frac{\partial\varepsilon}{\partial z}\right]$$
$$+C_{\varepsilon1}\frac{\varepsilon}{k}G-C_{\varepsilon2}\rho\frac{\varepsilon^2}{k} \quad (8)$$

The generation term (G) is written as, Ibrahim [9].

$$G=\mu_t\left[2\left(\frac{\partial u}{\partial x}\right)^2+\left(\frac{\partial u}{\partial y}\right)^2+\left(\frac{\partial u}{\partial z}\right)^2+\left(\frac{\partial v}{\partial x}\right)^2+2\left(\frac{\partial v}{\partial y}\right)^2+\left(\frac{\partial v}{\partial z}\right)^2+\left(\frac{\partial w}{\partial x}\right)^2+\left(\frac{\partial w}{\partial y}\right)^2\right.$$
$$\left.2\left(\frac{\partial w}{\partial z}\right)^2+2\left(\frac{\partial u}{\partial y}\frac{\partial v}{\partial x}\right)+2\left(\frac{\partial u}{\partial z}\frac{\partial w}{\partial x}\right)+2\left(\frac{\partial v}{\partial z}\frac{\partial w}{\partial y}\right)\right] \quad (9)$$

Where:

C_μ=0.09 ، σ_k=1.00 ، σ_ε=1.3 ، $C_{\varepsilon1}$=1.44، $C_{\varepsilon2}$=1.92

4. Numerical solution procedure

The solution is based on the following initial and boundary conditions.

Initial conditions

The velocity and temperature profiles were assumed uniform at entrance section and the transverse velocities variations are neglected at this section.

$$\left.\begin{aligned} u(0,y,z) &= u_{in} \\ v(0,y,z) &= 0 \\ w(0,y,z) &= 0 \\ T(0,y,z) &= T_{in} \\ P(0,y,z) &= P_{in} \end{aligned}\right\} \quad (10)$$

For turbulence parameters the following initial conditions are used, Ibrahim [9].

$$\left.\begin{aligned} k(0,y,z) &= k_{in} = C_k u_{in}^2 \\ \varepsilon(0,y,z) &= \varepsilon_{in} = C_\mu k_{in}^{3/2} / (0.5 D_h C_\varepsilon) \end{aligned}\right\} \quad (11)$$

Where C_ε and C_k are constants and given the following values $(C_\varepsilon = 0.03 \& C_k = 0.003)$ as indicated in Launder and Spalding [8]. D_h represents the hydrodynamic diameter, D_h =4A/PP.

Exit boundary conditions

At exit section the stream wise variation of velocity components and temperature are neglected.

$$\left.\begin{aligned} \frac{\partial u}{\partial x} &= \frac{\partial v}{\partial x} = \frac{\partial w}{\partial x} = 0 \\ \frac{\partial T}{\partial x} &= 0 \\ \frac{\partial k}{\partial x} &= \frac{\partial \varepsilon}{\partial x} = 0 \end{aligned}\right\} \quad (12)$$

Wall boundary conditions

The following wall boundary conditions are used.

$$\left.\begin{aligned} u(x,0,z) &= v(x,0,z) = w(x,0,z) = 0 \\ u(x,y_{max.},z) &= v(x,y_{max.},z) = w(x,y_{max.},z) = 0 \\ u(x,y,0) &= v(x,y,0) = w(x,y,0) = 0 \\ u(x,y,z_{max.}) &= v(x,y,z_{max.}) = w(x,y,z_{max.}) = 0 \end{aligned}\right\} \quad (13)$$

$$\left.\begin{aligned} T(x,y,0) &= T(x,y_{max},z) = T(x,y,z_{max}) = T_P, y \neq 0 \\ T(x,0,z) &= T_{ins}, 0 < z < z_{max.} \\ T(x,0,z) &= \frac{T_P + T_{ins}}{2}, z = 0, z = z_{max.} \end{aligned}\right\} \quad (14)$$

Different values for absorbing plate temperature have been used, (T_P = 80, 73, and 50 ^{O}C). It is assumed that the bottom wall temperature equal to the air inlet temperature.

Close to the wall the viscous effects predominate over turbulent ones and the variations of the flow properties are much steeper. Two methods for analyzing these regions are available which are the wall function method and the low Reynolds number –modeling method. The wall function method is used in this work.

The boundary conditions for the k-**ε** model are,

$$\left.\begin{aligned} k(x,0,z) &= \left.\frac{\partial \varepsilon}{\partial y}\right|_{y=0} = 0 \\ k(x,y_{max.},z) &= \left.\frac{\partial \varepsilon}{\partial y}\right|_{y=y_{max.}} = 0 \\ k(x,y,0) &= \left.\frac{\partial \varepsilon}{\partial z}\right|_{z=0} = 0 \\ k(x,y,z_{max.}) &= \left.\frac{\partial \varepsilon}{\partial z}\right|_{z=z_{max.}} = 0 \end{aligned}\right\} \quad (15)$$

The governing equations and boundary conditions are discredited using the control-finite volume method. The numerical solution is obtained using the SIMPLE algorithm. The convective and diffusive fluxes are approximated using the up wind scheme, which was a more judicious approximation than either a hybrid or power-law scheme. The grids size in (x, y, and z) are (60x20x20, 60x18x29, 60x16x31) nodes for the three duct configurations respectively. Typically, it took about 1500-2500 iterations to reach convergence.

5- Results and Discussion

The effect of the flowing parameters namely, the inlet temperature, absorber plate temperature, duct configurations, and mass flow rate, on the studied parameters are presented and discussed.

Figs (2-a, 2-b and 2-c) show the variation air temperature growth with dimensionless height $Y = y/y_{max}$ at centre line of the duct for different positions along the duct (the first configuration) .The absorber plate temperature is assumed to be $T_P = 73\ ^oC$ while the inlet air temperature is $T_{in} = 25$, 30, and 35^oC, the air mass flow rate is 0.109 kg/s. The figs indicate that the air temperature increases with (Y) until it reaches maximum value near the absorber plate (duct wall). The results show that the effect of inlet air temperature is to raise the starting point of growth but the trend of growth is approximately the same, for example at duct exit and Y=0.75 along the duct the air temperature is (38.9631, 42.5285, and $46.0717\ ^oC$) for inlet air temperature (25, 30, and $35\ ^oC$) respectively .

Figs (3-a, and 3-b), show the isothermal contours of air flow for the first duct configuration. The x-axis represents $Z = z/z_{max}$ while the y-axis represents the height of duct $Y = y/y_{max}$. The contours represent the dimensionless temperature (T^*), which is the ratio of local temperature to bulk temperature (T_b) .The figs represent the results for two locations along the duct, namely x = 1.5 and 4.5 m respectively. The wall temperature is assumed constant $T_P = 73^oC$, and the inlet air temperature is assumed to be $T_{in} = 25^oC$. The results are for a mass flow rate of 0.109 kg/s. The results show that the value of contour is higher than unity near the hot wall at all cross section and decreases towards the centre and base of the duct .However there is a closed loop (cold region) at the duct centre for the 1.5 m cross section since there is no enough time to heat the air. Further down the duct the loop disappears and the contours become open. The minimum value of the contours is near insulation (bottom wall).

The variation of bulk exit air temperature with inlet air temperatures for a mass flow rate of 0.109 kg/s is shown in fig (4) .The fig shows that the bulk exit air temperature increases with inlet air temperature since the initial temperature is higher. This result is for the first configuration.

Figs (5-a, and 5-b) show the effect of absorber plate temperature on air temperature growth along the duct height for the first configuration at locations x = 3.0 and 4.5 m along duct respectively. The mass flow of air is 0.109 kg/s and the inlet air temperature is $25\ ^oC$. The figs show that increases the absorber plate temperature increases the rate of temperature growth since the temperature gradient between the plate and the air increases which increases the rate of heat transfer to the air.

Fig (6) shows the effect of absorber plate temperature on the local bulk air temperature along the duct for the first configuration. The fig shows that the local bulk air temperature increases with the increase of absorber plate temperature. The increase of absorber plate temperature from 50 to 80 ^{o}C produces an increase in the bulk air temperature of 9.5 ^{o}C.

Fig (7-a) shows the effect of duct configuration on air temperature growth at duct exit. The mass flow is maintained constant for all configurations and equal to 0.109 kg/s. It is seen that the third configuration gives rapid temperature growth than the other two configurations since the air flows as a thin sheet between absorber plate and the insulation, which means a shorter path of heat transfer. Fig (7-b) shows the variation of local bulk temperature with duct length for different duct configurations. The mass flow of air is 0.109 kg/s and constant absorber plate temperature of 73 ^{o}C. For all configurations the local bulk air temperature increases with distance along the duct until the exit since more time is available for heat transfer. The figure also indicates that the air in the third configuration reaches the maximum possible exit temperature at short duct length.

Fig (8-a) illustrates the effect of duct configuration on pressure drop at a plate temperature of 73 ^{o}C and inlet air temperature of 25 ^{o}C. It is clear that the third configuration gives higher pressure drop due to shorter flow depth. Also the pressure drop increases with duct length. Fig (8-b) shows a comparison of the exit pressure drop obtained in present work with the results of Baa and Adam [15]. Both figures show good agreement in trends. The present study gives higher pressure drop due to longer duct length.

Figs (9-a, and 9-b) show the isothermal contours of air flow at duct exit for the second and third configurations for fixed mass flow rate, 0.109 kg/s, fixed inlet air temperature 25 ^{o}C ,and constant absorber plate temperature of 73 ^{o}C. It is clear that air is heated more uniformly in the third configuration where the bulk air temperature is higher than the other two configurations. At Z = 0.5 and Y = 1 the value of the dimensionless temperature T*=1.456 and 1.5239 for configuration 2, and 3 receptivity.

Fig (10) shows the effect of mass flow rate on air temperature growth at exit section. It is clear that the mass flow rate affects the air temperature growth significantly especially at low air flow rates .These results are for the first configuration. The plate temperature is 73 ^{o}C and the inlet air temperature is 25 ^{o}C. This is expected since low mass flow rate means larger temperature difference for same heat transfer.

Fig (11) shows the effect of air mass flow rate on local bulk air temperature along the duct length. As expected, as the air mass flow rate increases the local air temperature decreases. The plate temperature and the inlet air temperature are as in fig (10).

Fig (12) illustrates the variation of the pressure drop with duct length for different mass flow rates for the first configuration. It is shown that the pressure drop increases with mass flow rate and duct length. The conditions are as in fig (8).

6- CONCLUSIONS

The following conclusions can be drawn from this work,

1-Narrow duct configuration [low aspect ratio] is best suited for solar air heater design.

2-The increase in inlet air temperature by about 10 ^{o}C gives increases in the bulk exit air temperature by about 6.5 ^{o}C.

3-The increase in mass flow rate of air reduces the bulk exit temperature of air.

4-The increase of absorber plate temperature from 50 to 80^{o}C gives an increase in bulk air temperature by about 9.5 ^{o}C

5-Narrow duct configuration gives larger pressure drop.

References

[1] Zekai Sen.," Solar Energy Fundamentals and Modeling Techniques," Copyright 2008, by Springer.
[2] Ashish K. " Mathematical modeling of solar air heater with different geometries". A Master Thesis in Engineering, Department of Mechanical Engineering, University of Thapar, Patiala.
[3] Hossein Assefi and Atikol U., " Performance potential of flat plate solar air heaters in Tehran ". Proceeding of the 7th IASME/WSEAS International Conference on Heat Transfer, Thermal Engineering and Environment, 2009.
[4] Molero Villar, Cejudo N. and Lopez J.M. "Numerical 3D heat flux simulation on flat plate solar collector". Solar Energy, Vol 83, pp 1086-1092, 2009.
[5] Ho-Ming Yeh and Chii-Dong Ho, " Solar air heater with external recycle". Applied Thermal Engineering, Vol 29, pp 1694-1701, 2009.
[6] Nama S, et, al "Estimation and comparison of diffuse solar radiation over Iraq". Kufa Journal Vol 1, No 2, pp 153-174, 2010.
[7] Yass.N.K., "Design, Construction and Testing of a Solar Ai Heater" .A Master Thesis in Thermal Engineering, University of Babylon, College of Engineering, Dept. of Mech. Eng. 2011.
[8] Launder B. E. and Spalding D.B., (1974), "The Numerical Computation of Turbulent Flows," Computer Methods in Applied Mechanics Engineering, No3 PP. 269-289, 1974.
[9] Ibrahim, A.N., "Developing Turbulent Flow and Heat Transfer Through Rectangular and Circular Duct Cross Section,"M.sc. thesis Mechanical Engineering Department University of Babylon, (2005).
[10] Versteeg H.K. and Malalasekera W., "An introduction to Computational Fluid Dynamics-The Finite-Volume Method" Handbook , Longman, (1995).
[11] Ferziger, J.H. and Peric, M., "Computational Methods for Fluid Dynamics" 2nd edition, Springer-Verlag Berlin Heidelberg, (1997).
[12] Rapely, C. W., "Fluid and Heat Flow in Tubes of Arbitrary Cross-Section", Ph.D., Thesis University of London, U.K, (1980).
[13] Awbi H. B., "Ventilation of Building," E and FN Spon Inc, (1998).
[14] Hayder, M. K., "Numerical and experimental study of enhancement heat transfer in Roughened Ribbed Duct", Ph.D., Thesis University of Technology, January (2004).
[15] Yousef Baa and Adam N.M.,"Performance analysis for flat-plate collector with and without porous media"Journal of energy in south Africa.Vol.19 No.4 (2008).

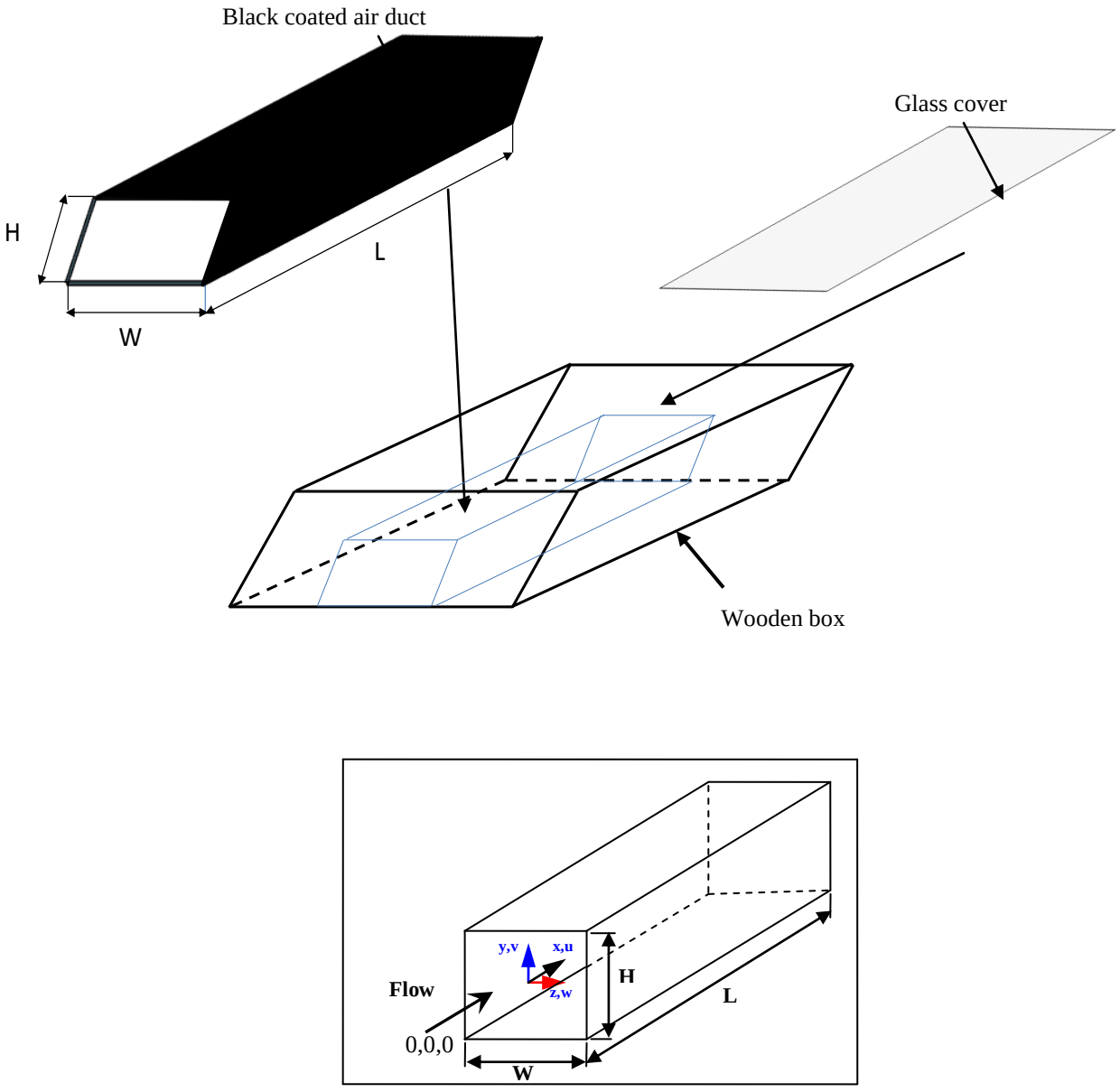

Fig (1) Schematic Representation of Solar Collector.

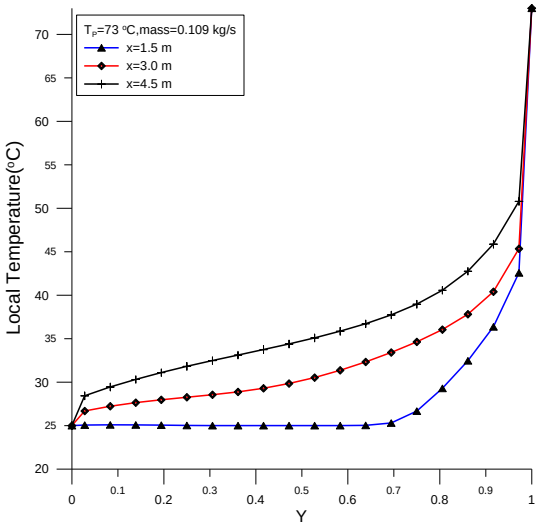

Fig (2-a) Variation of Air Temperature Along Duct Height for Different Duct Lengths (Tin=25 ^{o}C)

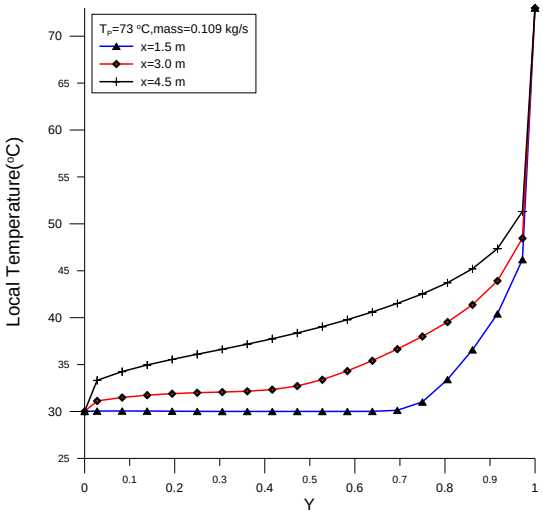

Fig (2-b) Variation ofAir Temperature Along Duct Height for Different Duct Lengths (Tin=30 ^{o}C)

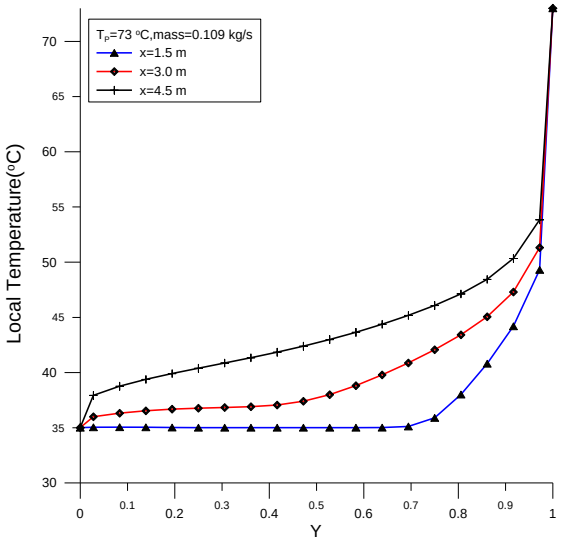

Fig (2-c) Variation of Air Temperature Along Duct Height for Different Duct Lengths (Tin=35 ^{o}C)

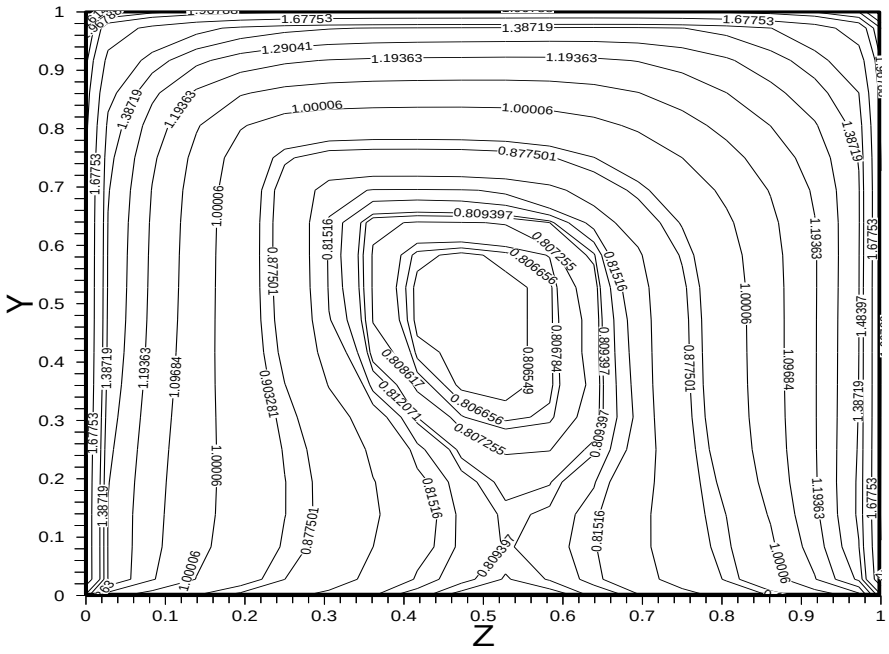

Fig (3-a) Isothermal Contours of Air at Duct Length of 1.5 m

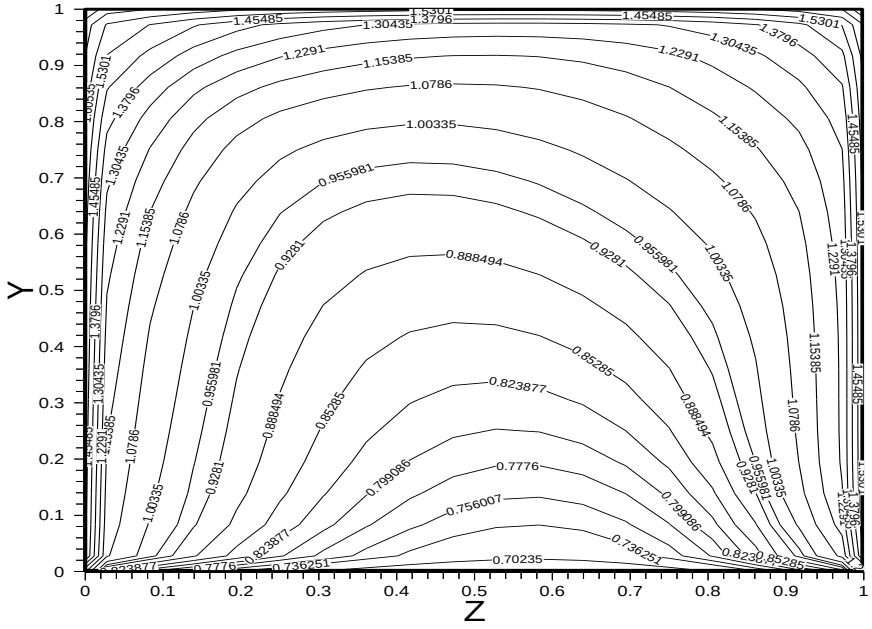

Fig (3-b) Isothermal Contours of Air at Duct Length of 4.5 m

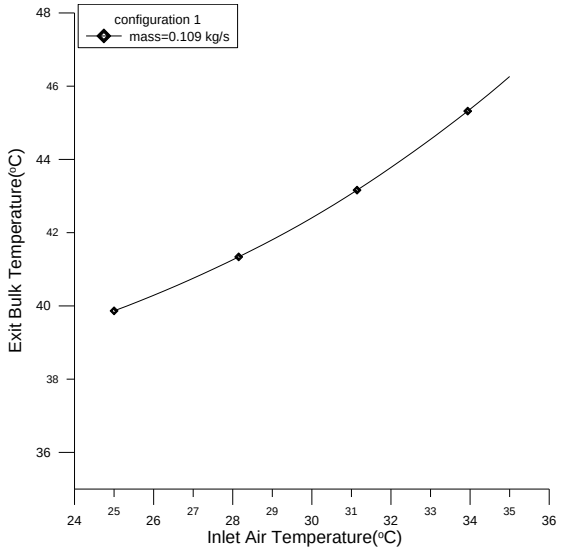

Fig (4) Variation of Exit Bulk Temperature With Inlet Air Temperature

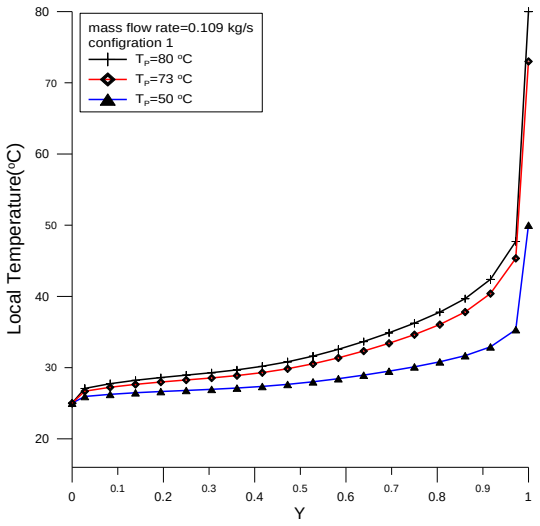

Fig (5-a) Variation of Air Temperature Along Duct Height for Differences Absorber Plate Temperature (x=3.0 m)

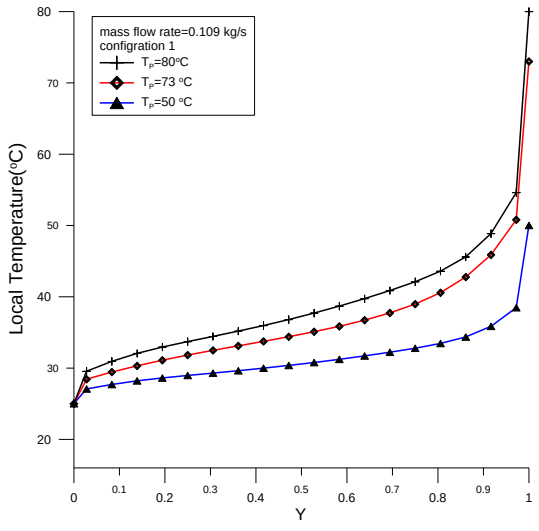

Fig (5-b) Variation of Air Temperature Along Duct Height for Differences Absorber Plate Temperatures (x=4.5 m)

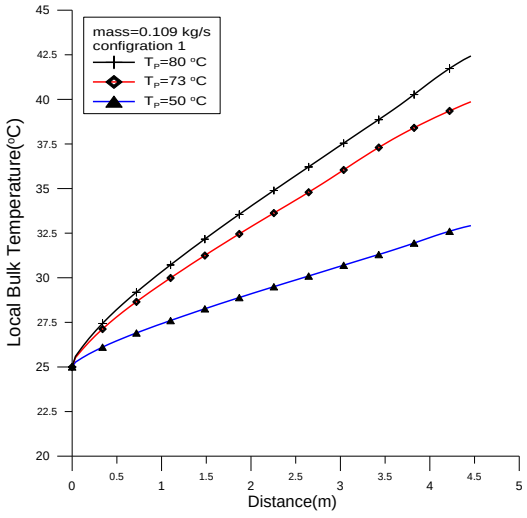

Fig (6) Variation of Local Bulk Temperature Along The Duct for Differences Absorber Plate Temperatures

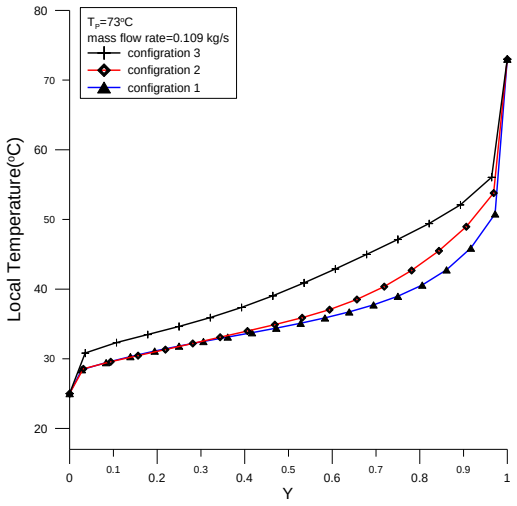

Fig (7-a) Variation of Air Temperature Growth for Different Configurations

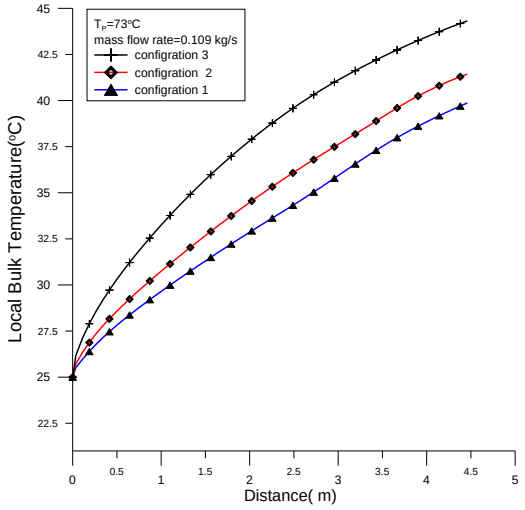

Fig (7-b) Variation of Bulk Temperature with Duct Length for Different Duct Configurations

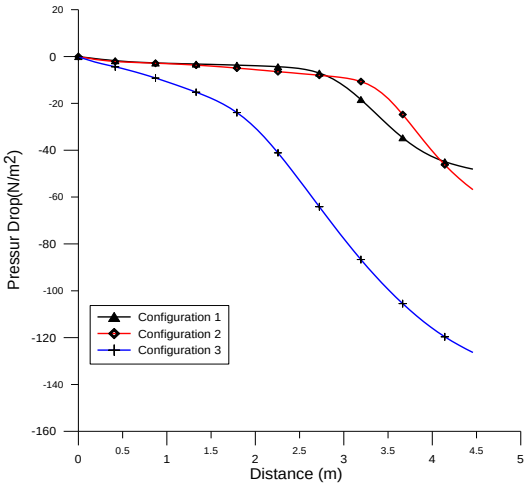

Fig (8-a) Variation of Pressure Drop Along the Duct for Different Configurations

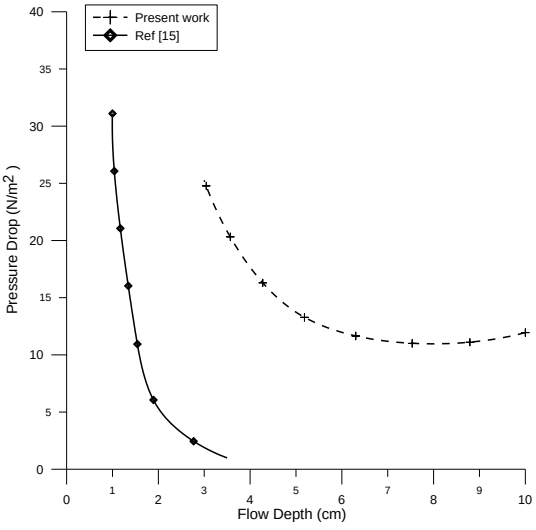

Fig (8-b) Comparison of Exit Pressure Drop Obtained in the Present Work With Results of .Ref[15].

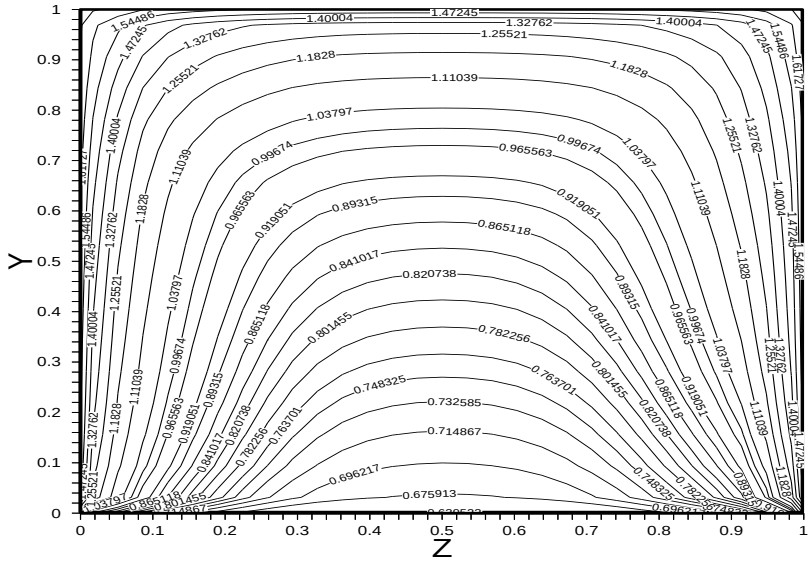

Fig (9-a) Isothermal Contours of Air for
Configuration 2 at Duct Exit

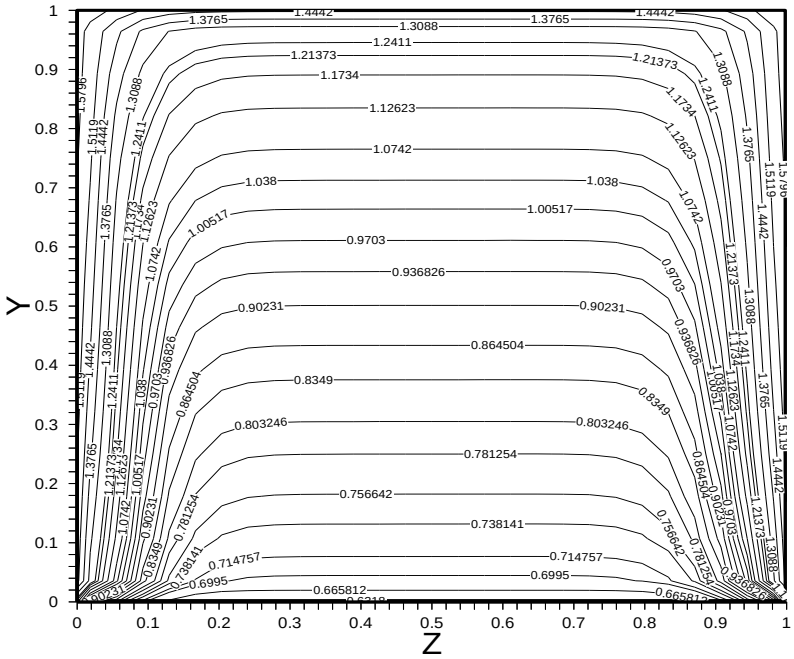

Fig (9-b) Isothermal Contours of Air for
Configuration 3 at Duct Exit

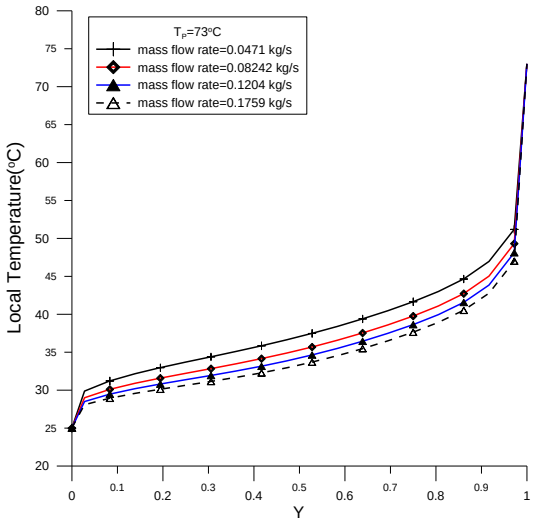

Fig (10) Variation of Air Temperature Along Duct Height for Different Mass Flow Rates

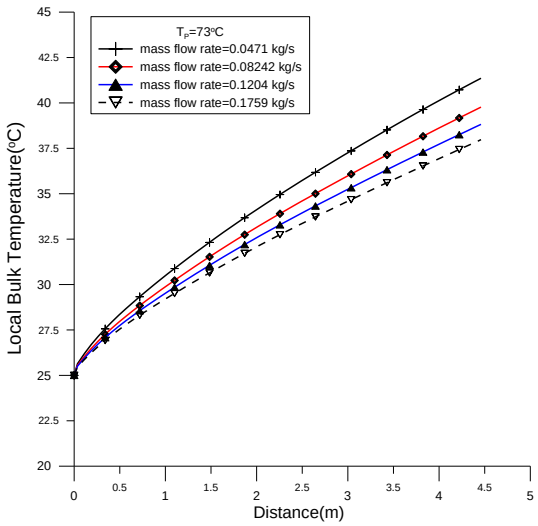

Fig (11) Variation of Local Bulk Temperature Along the Duct for Different Mass Flow Rates

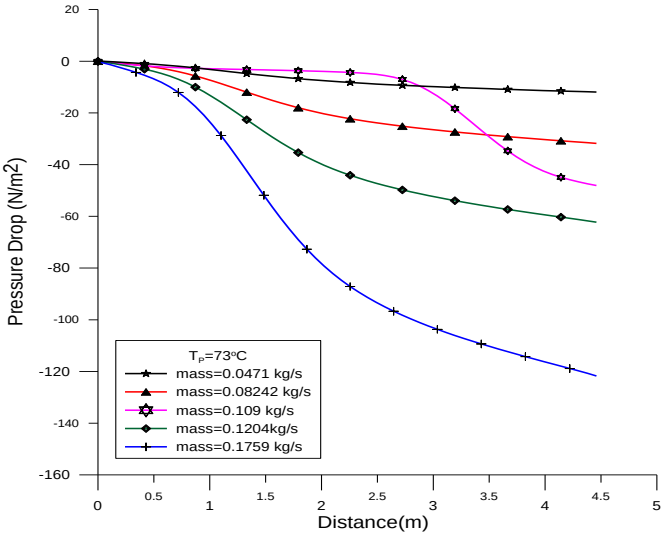

Fig (12) Variation of Pressure Drop Along the Duct for Different Mass Flow Rates